Estimation of Energy Expenditure in Wearable Healthcare Technology by Quantum-Based LSTM Modeling

(Invited Paper)

Bao-Nhi Dang Tran*, Muhammad Fahim†, Adnan Ahmad Cheema‡, Stephen Czarnuch*,
Bradley D. E. McNiven*, Octavia A. Dobre*, and Trung Q. Duong*

*Memorial University, Canada (e-mail: {ntrandangbao, sczarnuch, b.mcniven, odobre, tduong}@mun.ca)
†Queen's University Belfast, United Kingdom (e-mail: {m.fahim, trung.q.duong}@qub.ac.uk)
‡Ulster University, United Kingdom (e-mail: a.cheema@ulster.ac.uk)

***Abstract*—The quantification of physical activity energy expenditure (PAEE) offers significant benefits for healthcare monitoring and has the potential to promote healthy and active aging for elderly individuals. With recent advancements in quantum information and computation, quantum machine learning (QML) has emerged as a tool capable of improving upon the measurement of PAEE. In this paper, we propose a hybrid machine-learning model to predict PAEE. This model specifically leverages a classical long short-term memory (LSTM) model integrated with a variational quantum circuit (VQC). This model, which we refer to as the enhanced quantum long short-term memory linear (eQLSTML) model, was subsequently trained and tested using the publicly available GOTOV Human Physical Activity and Energy Expenditure Dataset for Older Individuals. Upon performance comparisons between the classical LSTM and proposed eQLSTML models, our findings suggest that the eQLSTML modeling approach demonstrates superior performance compared to classical machine learning methods, thereby holding a promise for personalized healthcare monitoring and promoting healthy aging in the older population.**

I. Introduction

Preserving health and functional mobility is paramount for maintaining a high quality of life, especially from the perspective of healthy aging. To date, there have been an increasing number of studies centered around the positive impacts regular moderate-intensity exercise has on older individuals, where the quantification and monitoring of physical activity energy expenditure (PAEE) was a key factor in promoting physical activity [1]. Moreover, additional work has shown that the measurement of indirect calorimetry through wearable accelerometer sensors is an affordable and effective method for PAEE estimation in older people [2]. More specifically, a combination of accelerometer data with physiological measurements (i.e., heart monitoring) has provided reasonable estimations on PAEE through linear and non-linear modeling methods. Furthermore, the application of deep learning methods has also been applied to the estimation of energy expenditure in individuals. For example, the application of artificial [3] and convolutional [4] neural network models have since been proposed to predict an individual's energy expenditure through wearable sensors. More recently, a recurrent neural network employing the use of a gated recurrent unit has been used to model PAEE in elderly individuals with high accuracy through the use of raw sensor and participant-level data [5].

In recent years, the development of quantum-based hardware and algorithms has led to a subfield of computing called quantum machine learning (QML). QML leverages the unique properties of quantum systems, such as superposition and entanglement, to develop novel algorithms for complex tasks beyond the capabilities of classical machine learning. One promising technique within QML is the variational quantum circuit (VQC) [6]. The VQC is a special type of quantum circuit where the parameters are tunable and optimized using classical algorithms to accomplish a desired outcome. This approach has shown promise in various applications in terms of expressive power by leveraging the fundamentals of quantum mechanics, with examples including quantum-based convolutional neural networks [7] and recurrent quantum neural networks [8]. In recent years, a quantum-based LSTM (QLSTM) model has been proposed for time series data, where VQCs have been used in place of the classical neural layer [9]. Other work [10] has proposed a linear-enhanced quantum LSTM (L-QLSTM) model, which utilizes a specialized embedding layer to achieve the input's dimension transformation to the expected output's dimension, for the practice of carbon price forecasting.

This paper proposes a novel hybrid enhanced quantum long short-term memory model which consists of a linear embedding layer, quantum angle embedding, and a variational quantum circuit (VQC). This model, which we refer to as eQLSTML, is applied to publicly available data and forecasts PAEE in elderly individuals. The main contributions of this paper are:

- The proposal of a hybrid quantum machine learning model that utilizes specialized data preprocessing of down-sampling using standard deviation aggregation to predict the PAEE for elderly individuals.
- Investigation the isage of VQCs with a controlled x-axis rotation gate (CRX), for stronger entanglement [11], and a circuit block connectivity pattern to offer better expressibility (i.e., the ability of the circuit to create pure states which are a good representation of the Hilbert space).

II. Dataset

In this work, experimental data was obtained from the Growing Old Together Validation (GOTOV) study which is open access through the 4TU data repository [12]. This dataset was specifically created to aid in the development of models for both activity recognition and energy expenditure estimation for an aging population [5], [13]. The dataset incorporates both indirect calorimetry measurements and data from accelerometers worn on different body locations such as the ankle and wrist.

A. Overview

The GOTOV study consists of 35 individuals (14 females, 21 males) mainly from Leiden, Netherlands who are between 60 to 85 years old. The statistical overview of participant-level data is shown in Table I.

TABLE I: Statistical information collected while performing 16 activities. SD - standard deviation, EEm - energy expenditure measurement, BMI - body mass index, BR - breathing rate.

	Mean	SD
Age	65.7	5.0
Height (cm)	174.5	7.9
Weight (kg)	83.1	11.5
BMI (kg/m)	27.2	2.7
EEm (Kcal)	3.8	1.1
BR (s)	0.31	0.04

In total, the participants engaged in 16 indoor and outdoor activities over a duration of 90 minutes. Indoor activities included resting postures (i.e., sitting and standing), stair climbing, and household chores (i.e., washing dishes, and vacuuming), while outdoor activities included walking at different paces and cycling. It is noted that only 25 participants were involved in outdoor activities due to weather limitations.

B. Devices and locations

The experiment used a set of devices that included an accelerometer and additional sensors to measure physiological signals like oxygen consumption, carbon dioxide production, breathing rate, and heart rate. We note that in this paper, we restrict our focus to data coming from accelerometers and indirect calorimetry.

Ankle and wrist-worn GENEActiv accelerometers captured the activity levels and movement patterns of the participants. These accelerometers recorded tri-axial acceleration data within an expected uncertainty of ± 8 g and a sampling rate of 83 Hz. Sample data from each accelerometer axis (ankle and wrist) is shown in Figure 1.

Indirect calorimetry measurements were performed using a COSMED K4b2 [14] system which measured breath-by-breath volumes of oxygen (O_2) and carbon dioxide (CO_2) throughout the activities, with a brief pause between indoor and outdoor sessions. The system includes a mask connected to a portable unit that housed O_2 and C_2 analyzers, barometric sensors, and processing electronics. These analyzers produced the measurement for O_2, and CO_2 exchange, allowing for the calculation of the energy expenditure measurement (EEm), along with metabolic equivalents. The EEm output served as our target variable for our PAEE modeling. Notably, the sampling rate of this signal matched the participant's breathing rate, resulting in a variable sampling rate averaging around 0.3 Hz.

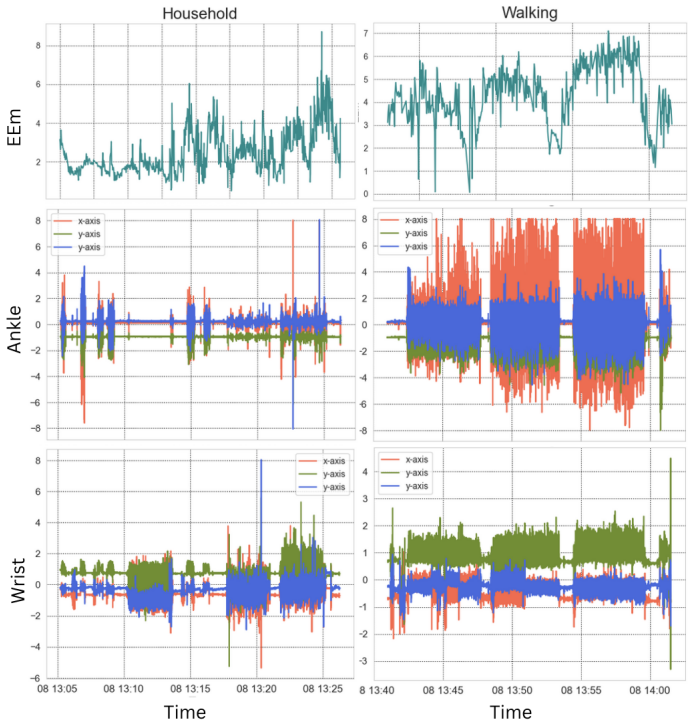

Fig. 1: Example showing raw data measured from ankle and wrist devices for household and walking.

III. Quantum circuits

A Quantum circuit is a sequence of quantum gates that perform a desired computation. These quantum gates operate on quantum bits (i.e., qubits), which exist in both the 0 and 1-bit states simultaneously via a superposition. This generalized state can be defined as

$$|\psi\rangle = \alpha|0\rangle + \beta|1\rangle \tag{1}$$

where α and β are the probability amplitudes of the $|0\rangle$ and $|1\rangle$ states, respectively, such that $|\alpha^2| + |\beta|^2 = 1$.

A. VQCs

VQCs are quantum circuits with adjustable parameters that can be optimized iteratively through parametrized quantum gates [15], and have gained attention due to their robustness against quantum noise in the ever-growing Noisy Immediate-Scale Quantum era [16]. To date, VQCs have been implemented in solving problems for a diverse range of areas, such as function approximation [6], quantum chemistry [17], generative modeling [18], and optimization [19]. Furthermore,

other work has shown stronger expressive power of VQCs in comparison to classical neural networks. Some noteworthy examples include the usage of a multi-parameterized quantum circuit as a simulator for probability distribution [20] and quantum annealing strategies coupled with entanglement methods in intractable classical problems [21].

In Figure 2, we present a simple circuit diagram of a VQC consisting of four qubits. As seen in the figure, the initial inputted states are set to $|0\rangle$ and proceed through the circuit to two unitary operations, where we assign x and θ as arbitrary parameters of their respective variational gate. Once these operations are completed, each qubit is then measured.

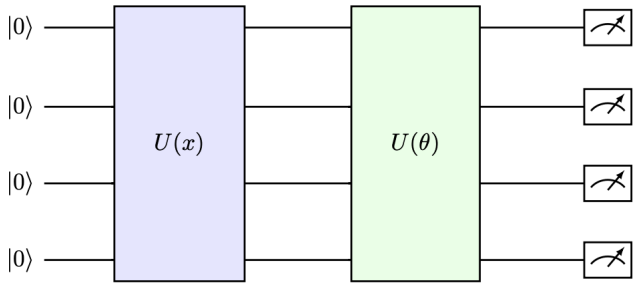

Fig. 2: Example of VQC architecture for a quantum circuit consisting of four qubits. U - unitary operation, x, θ - arbitrary variational gate parameter.

IV. Quantum Long Short-Term Memory and linear enhanced layers

Quantum Long-Short Memory (QLSTM) is a quantum-based version of the classical LSTM model, where the key distinguishing factor is the replacement of VQCs in different gates in the circuit. In QLSTM, the implementation of VQCs has been shown to play an essential role in the extraction of feature data and compression of data, along with the accelerated learning ability and enhanced stability for convergence [9].

A. Model Architecture

While QLSTM demonstrates effectiveness in time series forecasting with regular features, limitations arise due to qubit usage during the data encoding and compressing process. As QLSTM uses a one-to-one mapping scheme that requires encoding both hidden states (with p hidden units) and input features (with q features) to use $(p + q)$ qubits in VQC. However, the output dimension needs to be matched with the hidden state of q units, resulting in not only wasted quantum information for the remaining qubits during training but also to ineffective qubit usage that can hinder the model's learning ability. To combat this issue, a linear-layer embedding scheme was recently proposed which can significantly improve the QLSTM performance with effective usage of several qubits [10]. The linear embedding layer acts as a feature compressor, transforming input features with n-dimensions into a target dimension m using matrix multiplication. The feed-forward pass formulation is shown as:

$$z_t = L_e(v_t) \tag{2}$$
$$f_t = \sigma(L_1(VQC1(z_t))) \tag{3}$$
$$i_t = \sigma(L_2(VQC2(z_t))) \tag{4}$$
$$\tilde{c}_t = \tanh(L_3(VQC3(z_t))) \tag{5}$$
$$c_t = f_t \otimes c_{t-1} + i_t \otimes \tilde{c}_t \tag{6}$$
$$o_t = \sigma(L_4(VQC4(z_t))) \tag{7}$$
$$h_t = o_t \otimes \tanh(c_t) \tag{8}$$
$$y_t = L_o(h_t) \tag{9}$$

where L_e is the linear embedding layer applied to the concatenated vector, z_t represents the compressed output of a function of L_e, v_t, f_t, i_t, $\tilde{c}_t$, c_t, o_t, h_t, and y_t represent the forget gate, input gate, candidate cell state, cell state, output gate, hidden state, and output, respectively, at time step t. σ denotes the sigmoid activation function, and $\otimes$ represents element-wise multiplication. $\{L_m\}$ correspond to the set of linear layers applied after VQCs's output $m = (1, 2, 3, 4)$

Our proposed model takes into account this well-established embedding approach, but in different implementations. Specifically, our model employs separate feature embedding layers before and after each variational quantum layer instead of using a shared embedding layer before and a separate embedding layer after each VQC. These layers function as feature maps, transforming the input data vector v_t = $[h_t - 1, x_t]$ in which $h_t - 1$ represents the hidden state at the previous time step and x_t represents the current input into a compressed feature representation denoted as $z_{t,i}$ for VQC_i. This strategy of employing separate embedding layers allows for capturing non-linearities effectively and each layer can learn a distinct mapping specifically tailored to the corresponding VQC. This ultimately allows the model to better capture the intricacies of the data relevant to each quantum circuit. After the VQC layer, another separate embedding layer is used to map the VQC output to h_t. This preference stems from the analogy between VQCs in our proposed eQLSTML model and gates within a traditional LSTM. Similar to how distinct LSTM gates handle different functions, each VQC serves a specific purpose since a single, shared linear embedding layer wouldn't be able to effectively extract diverse information tailored to the unique functionalities of each VQC. Consequently, employing separate linear embedding layers after the implementation of the VQCs proves to be a more suitable approach, allowing the model to capture the nuances of the data relevant to each quantum circuit. We present a circuit diagram showing the implementation of our proposed eQLSTML model utilizing an enhanced layer embedding before and after VQCs in Figure 3.

B. VQC blocks

The VQC is comprised of three main components; the embedding layer, the variational layer, and the measuring layer. Quantum embedding refers to the process of encoding

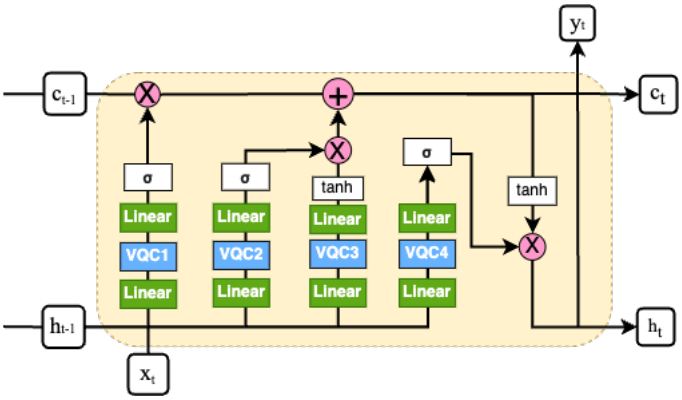

Fig. 3: Architecture of our proposed eQLSTML model with separate embedding layers before and after each VQC block.

classical data into its quantum representation. This embedding is done through a quantum feature map. The feature map acts as a translator converting classical data into a set of gate parameters, ultimately generating the corresponding quantum state. The quantum embedding technique used in the proposed model is angle embedding, which is the most prevalent encoding approach because of its simplicity and high efficacy [22]. In this encoding technique, the encoding process for classical input data x is done by single qubit rotation gates. Each element within the input vector determines the rotation angle of its corresponding gate (e.g., a rotation gate R_x). This encoding method requires n qubits or more to encode n input variables. Mathematically, this relationship can be expressed as:

$$|\psi_x\rangle = \otimes_n^i R_m(x_i)|\psi_0\rangle \tag{10}$$

where x is the classical input, R_m is selected rotation matrix in which $m = x, y, z$.

Within a VQC, the variational layer plays a pivotal role in achieving accurate learning. This variational layer performs the entanglement and rotation of qubits from a reference state to a target state that facilitates non-linear and complex information mapping. Hence, the variational layer's mapping properties are significant factors that influence the accuracy of prediction made by the Variational Quantum model. To achieve the optimal performance for the eQLSTML, this work proposes enhancements to the variational layer such as the usage of controlled X-rotation (CRX) for quantum entanglement techniques and circuit block for quantum bit connectivity patterns. The changes can improve the ordinary variational layer in the following ways. Firstly, the substitution of CRX gates allows quantum bits to take advantage of quantum entanglement as it allows the performance of variational rotations, and the quantum entanglement process, to happen at the same. Additionally, compared to the CNOT gate the circuit employing CRX is proved to exhibit superior expressibility and entangling capability. Furthermore, the CRX gates offer VQCs a larger effective number of parameters for the same number of gates which allows the circuit to explore a broader range of quantum states and more success in creating entanglement. Secondly, we used the circuit block connectivity between qubit pairs. The circuit block configuration is arranged in a natural way for a set of qubits to form a closed loop. More precisely, each circuit block within this structure incorporates regions of consecutive nearest-neighbor interactions complemented by a non-local interaction that establishes cyclic connectivity. This establishes increasing connectivity that can possibly lead to stronger entangling capacity and more relatively favorable expressibility while maintaining a lower cost of training in terms of circuit complexity and number of parameters [11].

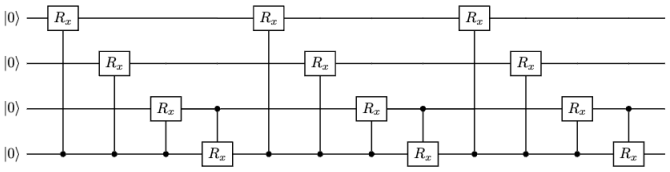

Fig. 4: Strongly entangled controlled-X CRX with circuit block connectivity interaction configuration in the proposed variational layer.

Lastly, the measurement layer is the measurement of each VQC block after the computational processes. In the proposed model, the measurement to be considered is computational basis state probabilities in Pauli-z operator. Expectation values can be computed numerically on classical computers through quantum simulator software packages that offer zero-noise quantum computation. However, on real quantum devices, these values are typically estimated statistically through repeated measurements. The measurement process yields a fixed-length vector and will be further processed by the classical computer for prediction purposes.

C. Optimization

Similar to classical machine learning models, the eQLSTML is trained to work with data-driven tasks. This learning process involves minimizing the loss function L(θ) also known as the objective function. In this paper, we used gradient-based algorithms to iteratively optimize VQC parameters. In this approach, the parameters are iteratively adjusted towards the direction that leads to the most significant decrease in the loss function, generally expressed as:

$$\theta_j \leftarrow \theta_j - \eta \nabla_{\theta_j} L(\theta) \tag{11}$$

where ∇_θ is the gradient and η is the learning rate.

The parameter-shift method, a type of forward-mode automatic differentiation [6], was employed in the optimization procedure to calculate the analytical gradient of the VQCs. The calculation for the gradient of a VQC following the parameter-shift method can be done via:

$$\nabla_\theta f(x,\theta) = \frac{1}{2}[f(x,\theta+\frac{\pi}{2}) - f(x,\theta-\frac{\pi}{2})] \tag{12}$$

where $f(x,\theta)$ is the output function.

D. Training and testing method

The training and testing process of our model employed the cross-validation method of leave one subject out (LOSO-CV)

to simulate model generalizability. In this approach, we train the model using data from all participants except for one that is left for the test set. This process is repeated to ensure all participants is tested separately. The LOSO-CV is used in order to minimize potential training set leakage that can occur in standard cross-validation techniques. Additionally, to monitor the performance of the model during the training process, a validation set comprising of two participants was used. These validation sets were randomly picked for each participant but stayed consistent across all model configurations to facilitate unbiased comparison.

V. Result and Discussion

This section will discuss our findings from experiments on the proposed model eQLSTML on a quantum circuit consisting of 6 qubits for the LSTM (see Figure 4). The performance will be compared with certain cases to provide comprehensive findings on how effective our proposed models are for energy expenditure prediction.

A. Performance of classical LSTM and proposed eQLSTML

Model performances are presented via averaged root squared error (R^2), root mean square error (RMSE), and mean absolute error (MAE) metrics. Test data sets consisting of 11 participants which performed all activities data were used to aid in the models ability to focus on core functionality and data efficiency.

TABLE II: Evaluation metrics of 11 participants for all activities for the eQLSTML and LSTM models.

	R^2	RMSE	MAE
eQLSTML	0.77	1.27	0.93
LSTM	0.69	1.49	1.15

Table II presents the performance metric comparison between the classical LSTM model and our proposed eQLSTML model. From the scores, our proposed eQLSTML outperformed classical LSTM in terms of all evaluation metrics. Specifically, the proposed model achieved a significantly higher R^2 score of 0.77 compared to the value of $R^2 = 0.69$ from LSTM, representing a 12% improvement. In terms of RMSE and MAE, the result for LSTMs is 1.49 and 1.14, respectively, while the eQLSTML model accomplished 1.25 and 0.93, respectively. The overall results show that our proposed model not only captures the underlying relationships within the data more effectively but also can make a closer approximation of actual values.

Figure 5 presents the performed energy expenditure predictions on the data by both eQLSTML and LSTM models and the testing data of one participant (labeled GOTOV12). The prediction of the eQLSTML architecture demonstrates a remarkable capability to capture the overall trend of both long-term and short-term time-series behaviors in the unseen (test) data set.

This is observed in the close gap between the predicted EEm values (red line) and the actual Eem values (blue line).

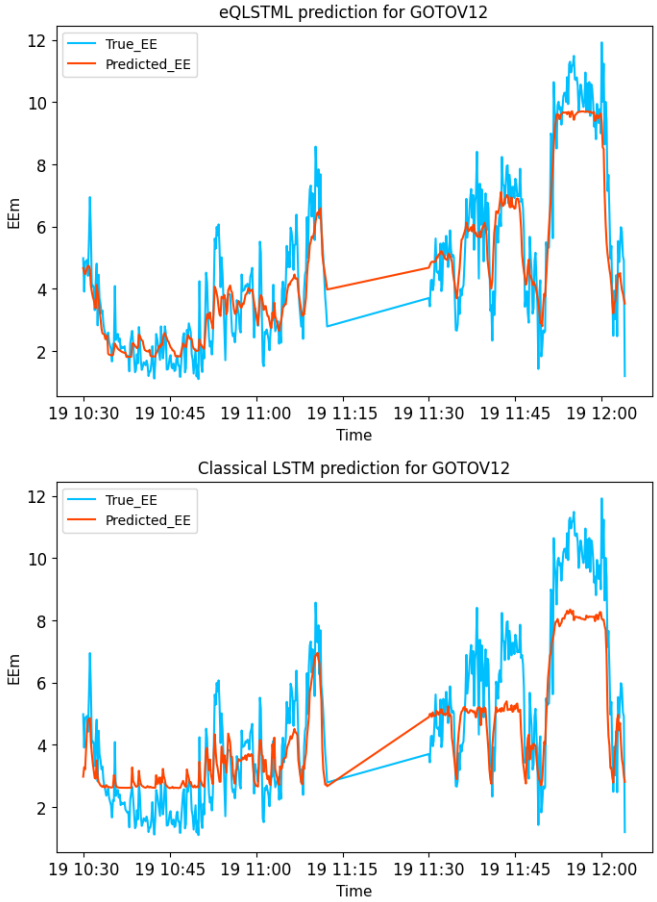

Fig. 5: True versus predicted values of EEm/breath for test participant GOTOV12, with indoor and outdoor activities included, generated by our eQLSTML model (top) and the classical LSTM model (bottom).

The eQLSTML sufficiently follows not only the changes of the blue line in the longer-term (true EEm) but also the short-term behaviors, including sudden changes indicated as high-low frequency fluctuations (i.e., the variant fluctuations from 11:00 to 11:15). In contrast, the classical LSTM model shows limitations in capturing the overarching temporal trends within the data and is incapable of following the longer-term changes. For example, it does not reflect the downtrend of the true value, especially in indoor activities with low intensity. Moreover, the models ability to make predictions for activities with high intensity is also quite lower than the true value, consequently leading to a significant deviation from the actual values compared to the results from eQLSTML. These observations suggest that the LSTM architecture might not be able to learn long-term dependencies effectively. Furthermore, our proposed eQLSTML model showed superior R^2, RMSE, and MAE metrics when compared to the classical LSTM model, as seen in Table III.

TABLE III: Evaluation metrics of the participant GOTOV12 for all activities for the eQLSTML and LSTM models.

	R2	RMSE	MAE
eQLSTML	0.87	0.98	0.77
LSTM	0.74	1.37	1.13

TABLE IV: Evaluation metrics of 11 participants for indoor activities for the eQLSTML and LSTM models.

	R2	RMSE	MAE
eQLSTML	0.43	0.90	0.67
LSTM	0.27	1.03	0.82

B. Comparative analysis of model performance for indoor and outdoor activities separately

In order to make a comprehensive comparison of our proposed models capability in terms of predicting low and high-intensity activities, we also evaluated the model with a test set that includes either indoor or outdoor activities and compared to results from the LSTM. Table IV presents evaluation metrics for indoor activities. From the tabulated data, the eQLSTML R^2 score is 0.43, which is $\sim 60\%$ higher than that of LSTM, which has a score of just 0.27. We also report a favorable decrease of 8% and 18% in the RMSE and MAE metrics from the eQLSTML model, with respective scores of 0.90 and 0.67.

TABLE V: Evaluation metrics of 11 participants for outdoor activities for the eQLSTML and LSTM models.

	R2	RMSE	MAE
eQLSTML	0.430	0.904	0.671
LSTM	0.266	1.031	0.824

Table V presents the same metric analysis from outdoor-specific activities. In this case, the eQLSTML model shows an R^2 score that is 25% higher than that from the classical LSTM case. Additionally, the eQLSTML again has smaller RMSE and MAE scores, with an overall decrease of 12% and 18%, respectively.

VI. Conclusion

In conclusion, this paper proposed a hybrid quantum machine learning model we call eQLSTML for predicting physical activity energy expenditure for the elderly. This model showed an improved learning ability compared to the classical LSTM model by leveraging the capabilities of quantum circuits for performing learning tasks more efficiently on sequential target data sets and was further optimized using variational quantum layers, strongly controlled-X gates for better entanglement, and angle embedding techniques. While this work demonstrates promising performance for the stated problem of PAEE in healthy aging, further research is necessary. We plan to extend this study and implement our proposed model on real quantum hardware to make a further comparative analysis of the model's effectiveness on other biosignal processing tasks. With further exploration, the eQLSTML model has the potential to unlock the power of quantum computation for complex learning tasks, especially in the field of healthcare signal processing.

Acknowledgment

This work was supported in part by the Canada Excellence Research Chair (CERC) Program CERC-2022-00109. The authors would like to acknowledge Xanadu Quantum Technologies for providing access to their PennyLane platform.

References

[1] T. M. Manini, J. E. Everhart, K. V. Patel, D. A. Schoeller, L. H. Colbert, M. Visser, F. Tylavsky, D. C. Bauer, B. H. Goodpaster, and T. B. Harris, "Daily Activity Energy Expenditure and Mortality Among Older Adults," *JAMA*, vol. 296, no. 2, pp. 171–179, 2006.

[2] W. R. Leonard, "Laboratory and field methods for measuring human energy expenditure," *American Journal of Human Biology*, vol. 24, no. 3, pp. 372–384, 2012.

[3] A. H. K. Montoye, M. Begum, Z. Henning, and K. A. Pfeiffer, "Comparison of linear and non-linear models for predicting energy expenditure from raw accelerometer data," *Physiological Measurement*, vol. 38, no. 2, p. 343, jan 2017.

[4] J. Zhu, A. Pande, P. Mohapatra, and J. J. Han, "Using deep learning for energy expenditure estimation with wearable sensors," in *2015 17th International Conference on E-health Networking, Application Services (HealthCom)*, Boston, USA, 2015, pp. 501–506.

[5] d. S. C. O. J. e. a. Paraschiakos, S., "A recurrent neural network architecture to model physical activity energy expenditure in older people." *Data Min Knowl Disc 36*, 2022.

[6] K. Mitarai, M. Negoro, M. Kitagawa, and K. Fujii, "Quantum circuit learning," *Phys. Rev. A*, vol. 98, p. 032309, Sep 2018.

[7] A. Ceschini, A. Rosato, and M. Panella, "Hybrid quantum-classical recurrent neural networks for time series prediction," in *2022 International Joint Conference on Neural Networks (IJCNN)*, Italy, 2022, pp. 1–8.

[8] B. B. S. K. N. S. Seth Aishwarya, Vaishnav Abeer, "Quantum computational techniques for prediction of cognitive state of human mind from eeg signals," *Journal of Quantum Computing*, vol. 2, no. 4, pp. 157–170, 2020.

[9] S. Y.-C. Chen, S. Yoo, and Y.-L. L. Fang, "Quantum long short-term memory," in *IEEE International Conference on Acoustics, Speech and Signal Processing (ICASSP)*, 2022.

[10] Y. Cao, X. Zhou, X. Fei, H. Zhao, W. Liu, and J. Zhao, "Linear-layer-enhanced quantum long short-term memory for carbon price forecasting," *Quantum Machine Intelligence*, vol. 5, jul 2023.

[11] S. Sim, P. D. Johnson, and A. Aspuru-Guzik, "Expressibility and entangling capability of parameterized quantum circuits for hybrid quantum-classical algorithms," *Advanced Quantum Technologies*, vol. 2, no. 12, p. 1900070, 2019.

[12] P. S. Paraschiakos, M. Beekman, A. Knobbe, R. Cachucho, and P. Slagboom, "Gotov human physical activity and energy expenditure dataset on older individuals." [Online]. Available: https://data.4tu.nl/articles/dataset/GOTOV_Human_Physical_Activity_and_Energy_Expenditure_Dataset_on_Older_Individuals/12716081, note={accessed:Nov.14,2023},

[13] J. Okai, S. Paraschiakos, M. Beekman, A. Knobbe, and C. R. de Sá, "Building robust models for human activity recognition from raw accelerometers data using gated recurrent units and long short term memory neural networks," in *2019 41st Annual International Conference of the IEEE Engineering in Medicine and Biology Society (EMBC)*, 2019, pp. 2486–2491.

[14] E. H. D. B. B. A. JE McLaughlin, GA King, "Validation of the cosmed k4 b2 portable metabolic system," *Int J Sports Med*, vol. 22, pp. 280–284, 2001.

[15] M. Cerezo, A. Arrasmith, R. Babbush, S. C. Benjamin, S. Endo, K. Fujii, J. R. McClean, K. Mitarai, X. Yuan, L. Cincio, and P. J. Coles, "Variational quantum algorithms," *Nature Reviews Physics*, vol. 3, pp. 625 – 644, 2020.

[16] M. Benedetti, E. Lloyd, S. Sack, and M. Fiorentini, "Parameterized quantum circuits as machine learning models," *Quantum Science and Technology*, vol. 4, no. 4, p. 043001, Nov. 2019.

[17] S. McArdle, S. Endo, A. Aspuru-Guzik, S. C. Benjamin, and X. Yuan, "Quantum computational chemistry," *Reviews of Modern Physics*, vol. 92, Mar. 2020.

[18] P.-L. Dallaire-Demers and N. Killoran, "Quantum generative adversarial networks," *Phys. Rev. A*, vol. 98, p. 012324, Jul 2018.

[19] S. E. Gaily and S. Imre, "Quantum optimization in large resource management systems," in *2019 IEEE 20th International Workshop on Signal Processing Advances in Wireless Communications (SPAWC)*, 2019.

[20] Y. Du, M.-H. Hsieh, T. Liu, and D. Tao, "Expressive power of parametrized quantum circuits," *Phys. Rev. Res.*, vol. 2, p. 033125, Jul 2020.

[21] T. Lanting, A. J. Przybysz, A. Y. Smirnov, F. M. Spedalieri, M. H. Amin, A. J. Berkley, R. Harris, F. Altomare, S. Boixo, P. Bunyk, N. Dickson, C. Enderud, J. P. Hilton, E. Hoskinson, M. W. Johnson, E. Ladizinsky, N. Ladizinsky, R. Neufeld, T. Oh, I. Perminov, C. Rich, M. C. Thom, E. Tolkacheva, S. Uchaikin, A. B. Wilson, and G. Rose, "Entanglement in a quantum annealing processor," *Phys. Rev. X*, vol. 4, p. 021041, May 2014.

[22] E. Ovalle-Magallanes, D. E. Alvarado-Carrillo, J. G. Avina-Cervantes, I. Cruz-Aceves, and J. Ruiz-Pinales, "Quantum angle encoding with learnable rotation applied to quantum–classical convolutional neural networks," *Applied Soft Computing*, vol. 141, p. 110307, 2023.